



Published in final edited form as:

*Acta Biomater.* 2019 January 01; 83: 177–188. doi:10.1016/j.actbio.2018.10.025.

## Development of keratin-based membranes for potential use in skin repair

Javier Navarro<sup>a,b</sup>, Jay Swayambunathan<sup>a,b</sup>, Max Lerman<sup>a,b</sup>, Marco Santoro<sup>a,b,\*</sup>, and John P. Fisher<sup>a,b,\*</sup>

<sup>a</sup>Fischell Department of Bioengineering, University of Maryland, 3121 A. James Clark Hall, College Park, MD 20742, United States

<sup>b</sup>Center for Engineering Complex Tissues, University of Maryland, 3121 A. James Clark Hall, College Park, MD 20742, United States

### Abstract

The layers in skin determine its protective and hemostasis functions. This layered microstructure cannot be naturally regenerated after severe burns; we aim to reconstruct it using guided tissue regeneration (GTR). In GTR, a membrane is used to regulate tissue growth by stopping fast-proliferating cells and allowing slower cells to migrate and reconstruct specialized microstructures. Here, we proposed the use of keratin membranes crosslinked via dityrosine bonding. Variables from the crosslinking process were grouped within an energy density (ED) parameter to manufacture and evaluate the membranes. Sol fraction, spectrographs, and thermograms were used to quantify the non-linear relation between ED and the resulting crosslinking degree (CD). Mechanical and swelling properties increased until an ED threshold was reached; at higher ED, the CD and properties of the membranes remained invariable indicating that all possible dityrosine bonds were formed. Transport assays showed that the membranes allow molecular diffusion; low ED membranes retain solutes within their structure while the high ED samples allow higher transport rates indicating that uncrosslinked proteins can be responsible of reducing transport. This was confirmed with lower transport of adipogenic growth factors to stem cells when using low ED membranes; high ED samples resulted in increased production of intracellular lipids. Overall, we can engineer keratin membranes with specific CD, a valuable tool to tune microstructural and transport properties.

---

\*Corresponding authors at: Fischell Family Distinguished Professor & Department Chair, Fischell Department of Bioengineering, University of Maryland, 4102A Clark Hall, 8278 Paint Branch Drive, College Park, MD 20742, United States (John P. Fisher). Fischell Department of Bioengineering, University of Maryland, 3121 Clark Hall, 8278 Paint Branch Drive, College Park, MD 20742, United States (Marco Santoro).

#### Declarations of Interest

JN, JS, ML, MS, and JPF declare no conflicts of interest.

#### Data availability

The raw/processed data required to reproduce these findings cannot be shared at this time as the data also forms part of an ongoing study.

#### Appendix A. Supplementary data

Supplementary data to this article can be found online at <https://doi.org/10.1016/j.actbio.2018.10.025>.

## Keywords

Keratin; Biomaterial; Hydrogel; Membranes; Guided tissue regeneration; Tissue stratification

---

## 1. Introduction

Severe skin burns are reported worldwide for over 11 million patients every year [1,2], including victims of violence (warfare [3], acid attacks [4,5], scalding [6]) and trauma [7] (flame, electrical, chemical). Skin is the first barrier against external mechanical and biochemical agents, and is composed of the epidermis, dermis, and hypodermis layers, each with its distinct composition and function. When burned, skin cannot regulate temperature or fluid transport, or stop bacterial infection [2,8]. Wound contraction after severe burns in adults is characterized by fast proliferation of fibroblasts that deposit random collagen to rapidly restore the skin barrier against external pathogens [9,10]. Depending on the size of the wound, as well as time and genetic factors, unsystematic deposition of extracellular matrix (ECM) and clotting can lead to scarred tissue [2]. This disorganized, fibrous tissue is characterized by lack of sensation and elasticity, hypertrophy, and flawed features; in effect, “natural healing” closes the wounds but does not restore skin function, layered microstructure, or aesthetic features [2,8–10]. Autologous grafting, the current gold standard [2,9,11,12], aims to restore the barrier using the patient’s skin but has the same limitations as wound contraction. It is imperative to develop strategies that restore the layered structure of native skin.

Toward this end, guided tissue regeneration (GTR) is a surgical technique developed for bone-related procedures in which a physical barrier is used to regulate tissue growth. Membranes are used to stop fast-proliferating fibroblasts and connective tissues from filling bone wounds, while allowing specialized cells (such as periodontal fibroblasts or bone cells) to migrate and correctly regenerate the osseous tissues [13–17]. Current GTR uses degradable membranes to restrict volumetric tissue growth and prevent cellular migration and unwanted deposition of ECM [15,16,18].

Here, we propose the use of crosslinked keratin membranes for GTR of skin. Keratins are a family of structural proteins that can be found either as a major cytoskeletal component of keratinocyte cells in the epidermis layers of skin (“soft” keratin) or as a fibrous extracellular protein in hair, wool, quills and horns (“hard” keratin) [19–21]. Keratin, particularly “hard” keratin, has been used in scaffolds and drug delivery carriers for skin [22], muscle [23], and nerve tissue engineering [23–29]. Furthermore, extracellular “hard” keratin has been successfully used in the treatment of dermal burn wounds on animal models (split-thickness burns in mice, rats [30], or pigs [31]) and on clinical patients (split-thickness burns <10% of total body surface area [22]). We previously reported a method for three-dimensional (3D) printing hair-derived keratin hydrogels using a riboflavin-sodium persulfate-hydroquinone (initiator-catalyst-inhibitor) photosensitive resin [32]. Ultra-violet (UV) light was used to form dityrosine bonds and photocrosslink keratin on a lithography-based 3D printer [32].

In this study we assessed the viability of UV-crosslinked keratin as a permeable membrane, particularly for the regulation of molecular transport. Under UV, the amount of energy

delivered to the resin volume (energy density, ED) defines the amount of dityrosine bonds formed and, correspondingly, the crosslinking degree (CD). As such, we hypothesize that ED could be used as a design parameter to control microstructural properties of the hydrogels, including swelling, degradation, mechanical properties, and transport across the network. First, we assessed if dityrosine bonding could be exploited to regulate the CD of keratin samples by controlling ED. We then quantified how CD affects properties dependent on the hydrogel microstructure, such as mechanical and swelling behaviors. As transport among dermal layers is fundamental for skin physiology, we were particularly interested in how the membranes can alter the diffusion rates of molecules towards a target cell population. As such, we studied the effect of CD on the partition coefficient and permeability of model molecules with varying molecular weights. Subsequently, we evaluated transport of growth factors and nutrients across the membranes and how engineered membranes can be used to regulate cellular functions, specifically adipogenic differentiation of mesenchymal stem cells.

## 2. Materials and methods

### 2.1. Keratin preparation

Keratin was prepared using a proprietary method by KeraNetics, LLC (Winston-Salem, NC). As described before [23,32], peracetic acid was used to oxidize human hair and keratin proteins were extracted using serial rinses with ultrapure water and Tris buffer, and purified by filtration and dialysis. Purified keratin was lyophilized, sterilized using gamma radiation, and stored at  $-20^{\circ}\text{C}$ .

### 2.2. Keratin resin and curing

The keratin-based photocrosslinkable resin was prepared as previously reported [32]. Briefly, keratin was dissolved overnight in phosphate buffered saline (PBS, pH 7.4) at a concentration of 4% wt/vol, and then mixed with a photosensitive solution at a 4:1 ratio. The photosensitive initiator-catalyst-inhibitor solution consisted of 1 mM riboflavin (Sigma-Aldrich Co., St. Louis, MO), 200 mM sodium persulfate (SPS, Sigma-Aldrich), and 0.001% wt/vol hydroquinone (Sigma-Aldrich), respectively. After thorough mixing the resin is curable under UV light by formation of dityrosine bonds as summarized in Fig. 1A. The crosslinking of keratin can be controlled with the UV light intensity ( $I$ ) [ $\text{mW}/\text{mm}^2$ ], exposure time ( $t$ ) [s], resin volume ( $V$ ) [ $\text{mm}^3$ ], exposed area ( $A$ ) [ $\text{mm}^2$ ], or sample thickness ( $h$ ) [mm]. These are the parameters we routinely control during our casting or printing processes. Here, we used them to define a unifying parameter, energy density (ED) [ $\text{mJ}/\text{mm}^3$ ], to produce, evaluate, and compare the hydrogels produced. The simplified function ED was defined as:

$$ED = (I \times A \times t)/V = (I \times t)/h \quad (1)$$

The resin was used to cast hydrogels using the ED parameter. For this, 3D printed molds were used, either with square ( $10 \times 10$  mm) or circular (8 or 13 mm diameter) holes passing through. A glass slide was clamped to the bottom of the mold, and the sealed molds were

then filled with resin as needed and exposed to UV at constant intensity [32] of 350 mW/dm<sup>2</sup>, defining the thickness of the sample using a known resin volume (Fig. 1B). Samples were rinsed and stored in PBS at 4°C. Nomenclature was defined as exposure time-thickness (e.g. Sample 12–1.5 is a sample with thickness of 1.5 mm, UV exposed for 12 min) (Fig. 1C and D).

### 2.3. Initiator consumption

Cylindrical samples (13 mm diameter, 1.5 mm thick) were exposed to UV for 6, 12, 24, 48, and 96 min as described in the previous section, producing samples groups 6–1.5, 12–1.5, 24–1.5, 48–1.5, and 96–1.5, respectively. These groups had ED values of 8.4, 16.8, 33.6, 67.2, and 134.4 mJ/mm<sup>3</sup>, as presented in Fig. 2A (further combinations of thickness and exposure time, and the resulting ED values, can be found in this graph). Samples were collected after casting and immediately stored in 20 ml excess PBS at 4°C in the dark for 4 days. Afterward, the conditioned PBS containing the uncrosslinked residues of the keratin resin was collected. 100 µl samples from each solution were set in 96 well-plates for absorbance reading of riboflavin at 450 nm using a SpectraMax M5 plate reader (Molecular Devices, Sunnyvale, CA). Control samples included unreacted resin, riboflavin, SPS, hydroquinone, and keratin, in PBS (n = 9). Absorbance of the samples was normalized against the unreacted resin control for quantitative comparison.

### 2.4. Sol fraction

Thick cylinder samples (8 mm diameter) 8–3, 24–3, 48–3, and 96–3 were prepared as described above. Samples were collected after casting and lyophilized without rinsing. Next, samples were weighed (unrinsed total mass) and stored in excess PBS at 4°C. The samples were then rinsed following our rinsing protocol (See Supplementary data Methods and Fig. S1). Briefly, sequential rinses using fresh PBS for 15 min, at room temperature, for a total of 9 cycles; a final tenth rinse was a single, extended overnight rinse (14 h). All samples were then lyophilized again and weighed (rinsed mass), using a microbalance (Sartorius ME-5, Sartorius, Goettingen, Germany). The sol fraction [%] of the sample was calculated as the difference between the unrinsed total mass and the rinsed mass, over the total mass (n = 12).

### 2.5. Fourier-Transform infrared spectroscopy (FTIR)

Thin membrane samples (10 × 10 mm) 12–1.5, 24–1.5, 48–1.5, and 96–1.5 were prepared as described above. After completing the rinsing protocol in PBS and lyophilization, samples were mounted onto MirrIR Low-e Microscope Slides (Kevley Technologies, Chesterland, OH). FTIR measurements were performed on a Smiths IlluminatIR II, imaging under attenuated total reflection (ATR) mode. 100 × 100 µm sampling areas were scanned 128 times per sample. Background was removed and the diamond contact probe cleaned with 100% ethanol before each sample. Control samples included uncrosslinked keratin, PBS, and photosensitive solution only (n = 9). Quantification of the peaks was done by taking the area under the curve within the 1400 to 1650 cm<sup>-1</sup> range and normalizing against the value for unreacted keratin. Variations in these results were used to assess alterations in the aromatic rings of tyrosine due to the formation of dityrosine bonds. Post-processing of FTIR spectra was done using Spectragryph – optical spectroscopy software [33].

## 2.6. Thermogravimetric analysis (TGA) and differential scanning calorimetry (DSC)

Thin membrane samples (10 × 10 mm, 1.5 mm thick) 12–1.5, 24–1.5, 48–1.5, and 96–1.5 were prepared as described above. Additional samples for 12–2 and 96–1 groups were prepared, representative of low and high ED, respectively. All samples were subjected to our standard rinsing protocol in PBS and then lyophilized. The 12–2 and 96–1 samples, and uncrosslinked lyophilized keratin, were subjected to thermogravimetric analysis (TGA, TA Instruments, New Castle, DE - Energy Research Center, University of Maryland) heating the samples up to 350 °C at 10 °C/min under 100% N<sub>2</sub>. TGA was performed to identify variations between crosslinked and uncrosslinked samples, and to determine the temperature ranges where these occurred. The 1.5 mm thick samples, and uncrosslinked keratin controls, were massed using a micro-balance (Sartorius ME-5, Gottingen, Germany) and sealed into differential scanning calorimetry (DSC) pans (10–15 mg per pan). DSC was performed on a Q100 differential scanning calorimeter (TA Instruments, New Castle, DE) by heating the samples from 30 to 300 °C at 10 °C/min under 100% N<sub>2</sub>. Resulting thermograms were compared to those of uncrosslinked controls to determine the crosslinking degree (CD) as previously reported in literature [34] (n = 9–15). Briefly, in DSC thermograms the area under the peak represents the maximum enthalpy change possible in the system. Changes in these areas are indicative of changes in the internal energy of the network and are used to quantify bond formation and CD. As such, enthalpy change was used to calculate CD [34], as:

$$CD(S_x)[\%] = \frac{\Delta H(S_0) - \Delta H(S_x)}{\Delta H(S_0)} \times 100 \quad (2)$$

where,  $H(S_0)$  is the reaction enthalpy of uncrosslinked reference (area under reference peak) and  $H(S_x)$  is the reaction enthalpy of the crosslinked sample (area under sample peak).

## 2.7. Swelling

Thin membrane samples (10 × 10 mm) were prepared for the combinations 12–2, 12–1.5, 12–1, 24–2, 24–1.5, 24–1, 48–2, 48–1.5, 48–1, 96–2, 96–1.5, and 96–1. All samples were rinsed in PBS over 24 h following our standard protocol and then lyophilized. Initial dried mass was recorded. The samples were then rehydrated in 2 ml excess minimum essential medium (MEM, Life Technologies, Frederick, MD) at 37 °C. Rehydrated mass of the samples was recorded at 1, 3, 5, 10, 15, 20, 30, 45, and 60 min, 3 h, 6 h, 24 h, 2d, 3d, 5d, 7d, 14d, 21d, and 28d. At each time point the sample was taken out of solution, gently blotted to remove excess MEM, weighed (swollen mass), and then returned to the solution. The volume of MEM was kept at 2 ml by refilling every 3 days. Swelling was calculated as the difference between swollen mass and dried mass, over dried mass (n = 9).

## 2.8. Mechanical properties

Thick cylinder samples (8 mm diameter) 8–4, 24–4, 48–4, and 96–4 were analyzed using an Instron 5565 (Instron, Norwood, MA). Mechanical compressive testing was done on the samples using a 50 N load cell at a compression rate of 1 mm/min until yielding. The

ultimate stress and strain values were taken from the stress–strain curves, and the linear regime of the curves was determined with a linear fit ( $R^2 = 0.95$ ) to obtain the compressive modulus ( $n = 7$ ).

## 2.9. Partition coefficient

Thin membrane samples (13 mm diameter), 12–1.5, 24–1.5, 48–1.5, and 96–1.5 were rinsed following our standard protocol and then equilibrated in PBS at room temperature for an additional 24 h. Separately, fluorescein isothiocyanate-dextran (FITC<sub>d</sub>, 10, 150, or 2000 kDa molecular weight (MW)) was dissolved at 10 mg/ml in PBS, and equilibrated under the same conditions. Samples from the initial FITC<sub>d</sub> solutions were taken and measured for fluorescence in the SpectraMax M5 plate reader. The mass of equilibrated hydrogels was also recorded. The hydrogels were then removed from the PBS and added to 0.5 ml of the equilibrated FITC<sub>d</sub> solutions. After 24 h, 10  $\mu$ l samples were collected from the solutions and diluted with 90  $\mu$ l of PBS. Samples were read for fluorescence alongside a FITC<sub>d</sub> concentration ladder, to calculate the concentration of the sampled solutions ( $n = 9$ ). The partition coefficient (K) is the steady-state relation between the concentration of a solute in a gel ( $C_g$ ) and the concentration of the solute in the solution ( $C_s$ ) in which the gel is equilibrated in. As such, K between crosslinked keratin and the FITC<sub>d</sub> solutions was obtained using the mass balance of the FITC<sub>d</sub> between the hydrogel and the solution [35], which results in:

$$K = \frac{C_g}{C_s} = \frac{V_s(C_i - C_f)}{V_g C_f} \quad (3)$$

where  $C_i$  is initial concentration of FITC<sub>d</sub> in solution;  $C_f$  is stable final concentration of FITC<sub>d</sub> in solution;  $V_s$  is volume of solution; and  $V_g$  is volume of the hydrogel, which is assumed equal to the equilibrated mass of the hydrogel as it is over 95% PBS (density  $\sim 1$  g/ml).

## 2.10. Permeability

Thin membrane samples (13 mm diameter), 12–1.5, 24–1.5, and 96–1.5 were prepared as described above, rinsed following the protocol, and equilibrated in PBS at room temperature for over 24 h. Thickness and diameter of the equilibrated membranes was recorded before setting them in Transwell inserts (Falcon<sup>R</sup> Permeable Support for 12 Well Plate with 8  $\mu$ m transparent polyethylene terephthalate (PET) membrane, Thermo Fisher Scientific, Waltham, MA). The PET membrane of the Transwell was punctured five times using a 22G 1½ needle to guarantee that any barrier effect was due to the keratin membrane. 3D printed stoppers are used to weigh down the membrane and assure sealing. The well (receiver side) was filled with 1.3 ml of PBS and allowed to re-equilibrate with the membrane for 12 h. After, 1.3 ml of 10 mg/ml FITC<sub>d</sub> solution (10, 150, or 2000 kDa MW) in PBS was added to the Transwell (donor side) at room temperature. At 0, 5, and 30 min, and 1, 2, 3, 6, and 24 h, a 5  $\mu$ l sample was collected from the donor and receiver sides and diluted with 95  $\mu$ l of PBS. Three samples were tested per FITC<sub>d</sub> solution, alongside a FITC<sub>d</sub> concentration ladder ( $n = 9$ ). Volume loss in the wells was 5.4 to 8.1%, thus we assumed constant volume and

concentrations throughout the test. We further assumed that the donor had known initial concentration while the receiver concentration was zero, and that flux across the membrane quickly reaches steady state and does not change over time. As such, we used a pseudo-steady state model, in which the concentration profile across the membrane is assumed invariant, to calculate the permeability (P) of the hydrogels to each type of FITCd by plotting [36]:

$$-\ln\left(\frac{C_d - C_r}{C_{d0} - C_{r0}}\right) = \left(\frac{PtA}{L}\right)\left(\frac{1}{V_d} + \frac{1}{V_r}\right) \quad (4)$$

where  $C_d$  is donor concentration at time  $t$ ;  $C_r$  is receiver concentration at time  $t$ ;  $C_{d0}$  is initial donor concentration;  $C_{r0}$  is initial receiver concentration;  $t$  is time;  $A$  is membrane area;  $L$  is membrane thickness;  $V_d$  is donor volume; and  $V_r$  is receiver volume.

### 2.11. Transport of adipogenic molecules across keratin membranes

Thin membrane samples (13 mm diameter), 12–1.5, 24–1.5, and 96–1.5 were cleaned following our protocol for sequential PBS rinses and equilibrated in PBS at room temperature for over 24 h. The membranes were used in Transwell inserts with stoppers using the same methodology described above. Human mesenchymal stem cells (hMSCs, Lonza, Walkersville, MD) were seeded in 12-well cultures plates at a density of 5000 cells/cm<sup>2</sup> and expanded to total confluence, as suggested by the provider for successful adipogenesis, by feeding them every 3 d with hMSC growth media (Dulbecco's Modified Eagle Medium (DMEM) with 10% fetal bovine serum (FBS), 1% non-essential amino acids (NEAA), and 1% penicillin/streptomycin 100 U/100 mg (P/S)). Once at total confluence, the Transwell-membrane setups were set on the culture wells. The Transwell donor side was filled with 0.5 ml of hMSC adipogenic media (DMEM with 10% FBS, 100 U/100 mg P/S, 1 mM sodium pyruvate, 1 μM dexamethasone, 10 mg/ml insulin, 0.5 mM 3-isobutyl-1-methylxanthine (IBMX), and 200 mM indomethacin) [37,38], while the receiver side with the cells was filled with 0.5 ml hMSC growth media. Media on both sides was replenished every 3d for 21d. As positive controls, wells with Transwell only or no Transwell were fed with 1.5 ml of adipogenic media, while negative controls without Transwell or membrane, were fed hMSC growth media to avoid differentiation. Adipogenic differentiation of hMSCs was assessed after 21d using AdipoRed™ Assay Reagent (Lonza) to quantify intracellular lipid accumulation (n = 9).

### 2.12. Statistics

Statistics for quantitative tests were performed using ANOVA and Tukey's multiple pairwise comparison (significance using  $p < 0.05$ ) for multi-group comparisons. Differences between individual groups and references were assessed with two-sample  $t$ -test for the mean (significance using  $p < 0.01$  (+) and  $p < 0.05$  (\*)).

### 3. Results

The goal of this work was to prove that dityrosine bonding chemistry could be used to engineer keratin membranes and to regulate molecular transport. As hypothesized, the energy density during the curing process was used as a design parameter to control the hydrogel's physicochemical properties, including permeability across the membrane. As illustrated in Fig. 1, the keratin photosensitive resin and the tyrosine available in oxidized keratin were successfully exploited to produce hydrogels. The ED parameter proposed (Eq. (1)) was used to produce a variety of crosslinked samples by combining different thicknesses and exposure times. As shown in Fig. 2A, samples ranged from low ED ( $6.3 \text{ mJ/mm}^3$  minimum) to high ED ( $201.6 \text{ mJ/mm}^3$  maximum). Samples within this range were used to assess how the crosslinking density (CD) of keratin could be regulated using the ED parameter.

The extent of crosslinking of the resin was assessed by quantifying the uncrosslinked tyrosine residues within the hydrogels, and by measuring the CD of the samples. Unreacted riboflavin content was found to decrease as the ED increased (Fig. 2B), indicating that the chemical initiation does occur. For the lowest ED sample ( $8.4 \text{ mJ/mm}^3$ ) the initiator residue was 72% the initial amount, while the highest ED sample tested ( $134.4 \text{ mJ/mm}^3$ ) had residues as low as 1.4%. The riboflavin initiator is mostly consumed when crosslinked with a  $67.2 \text{ mJ/mm}^3$  ED (12% of the initial riboflavin is left unreacted) and close to absolute consumption with  $134.4 \text{ mJ/mm}^3$ . The sol fraction of the samples was also decreased in a non-linear trend as the ED increased (Fig. 2C); here, the decrease in sol fraction fell within a narrow range (73.2–68.6%), yet the differences between groups were significant ( $p < 0.05$ ). Both sets of data were acquired on samples that had thoroughly completed the rinsing protocol, after which no leachable products should be left in the hydrogels (See Supplementary data and Fig. S1). All subsequent sets of data were rinsed following the same protocol to avoid soluble leaching confounding in the results. FTIR spectra (Fig. 2D) showed four characteristic peaks at 1400, 1450, 1525, and  $1650 \text{ cm}^{-1}$  which are representative of C = C stretch patterns in the rings of aromatic compounds (Fig. 1A); the comparison between groups and the uncrosslinked control showed significant changes dependent on the ED (Fig. 2E).

TGA (Fig. 2F) performed on representative samples of low and high ED showed that profiles of crosslinked samples differed from the unreacted reference within a temperature range of 150 to 275 °C. DSC showed a characteristic peak (around 200 °C) in the uncrosslinked keratin profile; for crosslinked samples the peak shifts to 220–230 °C and changes in magnitude depending on the ED (Fig. 2G). All samples present a defined peak, but as the ED increases the peak progressively disappears. As described in the Methods and Eq. (2), the changes in potential energy, enthalpy, were used to calculate a DSC CD for the samples. As illustrated in Fig. 2H, there is non-linear relation between ED and CD; the CD increases as ED increases at lower values until it reaches saturation point between 33.6 and  $67.2 \text{ mJ/mm}^3$ , after these values all samples have a maximum CD close 60%. From this, it was determined that samples with ED of 16.8, 33.6, 67.2, and  $134.4 \text{ mJ/mm}^3$  had a CD of 19.6, 46.9, 54.6, and 59.5%, respectively.

The swelling of crosslinked samples in MEM was studied over the period of 1 month. As presented in Fig. 3A, keratin hydrogels had a swelling capacity that varies around 1500% and was heavily determined by the ED of the sample. Swelling profiles showed a rapid increase during the first day and then a period of relative stability during the first 5 days. Stable swelling was determined at day 3, the point where most groups present either stability or a maximum peak (Fig. 3A and B). For the early time points, the low ED samples had a higher swelling degree, quickly reaching peak values  $2117 \pm 148$ ,  $1969 \pm 43$ , and  $1735 \pm 99\%$  (25.2, 16.8, and 12.6 mJ/mm<sup>3</sup> groups, respectively). The high ED groups (above 67.2 mJ/mm<sup>3</sup>) took longer to hydrate but remained consistently stable at their peak values throughout the 28 d. Here, we considered that the system reached the maximum CD with 67.2 mJ/mm<sup>3</sup> of ED, the level at which the swelling capability no longer increased ( $p < 0.05$ ). After 5d rehydrating, Fig. 3B shows how low ED groups had a significantly relevant drop in the swelling capacity ( $p < 0.01$  and  $p < 0.05$ ), registering drops as steep as  $-81 \pm 10\%$  (16.8 mJ/mm<sup>3</sup>) and  $-40 \pm 13\%$  (33.6 mJ/mm<sup>3</sup>). On the other hand, high ED groups with at least 67.2 mJ/mm<sup>3</sup> had no reduction in their swelling capacity (changes are not significant or increasing,  $p < 0.05$ ), indicating that these groups remained stable after 28d. The effects of lyophilization on the rehydration process of keratin-based hydrogels were studied to assess changes in diameter, thickness, and mass uptake. These studies showed some degree of irreversible frustration due to the drying process, which is the reason all subsequent studies were performed on samples that were always kept hydrated in PBS (See Supplementary data and Fig. S2).

The stress–strain curves for the crosslinked keratin samples (Fig. 3D) showed different behaviors dependent on the ED of the groups. As exposure time increases and sample thickness decreases, the materials become stiffer. This observation was further confirmed by quantifying the compressive modulus as a function of ED (Fig. 3D, inset). Additionally, as ED increases the ultimate stress increases and the ultimate strain decreases until both trends reach plateau levels (Fig. 3E). The trends here confirm that the hydrogel networks keep changing with ED up to 67.2 mJ/mm<sup>3</sup>; after that threshold, the mechanical properties measured reach their maximum values. Using the plateau of the plots, the ultimate stress registered for these groups was  $18 \pm 2$  kPa, while the ultimate strain was  $59 \pm 3\%$ .

Transport properties were studied to assess the viability of crosslinked keratin as membranes. The relation between ED and the partition coefficient (K) and permeability (P) of the hydrogels was studied using FITCd as a model molecule (Fig. 4A). For high MW of FITCd (150 and 2000 kDa) there was minimal or no variation of K as ED increased, while the low MW 10 kDa solution presented a sharp increase and subsequent increments of K as ED increased (Fig. 4B,  $p < 0.05$ ). On the other hand, the relation between ED and P had different trends. For the low MW (10 kDa) solutions, changes in the ED cause no significant variations in the P of the system ( $p < 0.05$ ); differently, for the high 150 and 2000 kDa MW samples there is continuous increase of K as ED increases (Fig. 4C). The overall increase in P between the low (16.8 mJ/mm<sup>3</sup>) and high (134.4 mJ/mm<sup>3</sup>) EDs was 28% (not significant), 289%, and 2576% for the 10, 150, and 2000 kDa solutions, respectively.

The transport of physiologically relevant molecules was studied with the diffusion of adipogenic media across the membranes. As observed in Fig. 4D, feeding the cells through

membranes with 20 and 47% CD resulted in sparse production of intracellular lipid vesicles in comparison with the more homogeneous production of populations fed through membranes with 55 and 59% CD. Quantification of these production levels (Fig. 4E) shows that all membrane groups allowed adipogenic differentiation of hMSCs. Within the study groups, membranes with 55 and 59% CD were linked to increased lipid deposition, 5–8 times greater than the non-differentiated controls, in comparison to the 20 and 47% CD ( $p < 0.05$ ).

## 4. Discussion

Membranes have been used in guided tissue regeneration (GTR) to regulate tissue growth. This technique is based on the idea that a physical barrier is needed to stop fast-proliferating cells (such as fibroblasts) from colonizing open wounds, while giving time to the slower specialized cells to migrate and regenerate particular microstructures of native tissues [13–17]. This is a common strategy in the treatment of periodontal diseases and enossal dental implants [13], as well as the treatment of critical-sized bone defects [15] and the preservation of empty sockets [14]. Current membranes provide biocompatibility, prevention of cell migration, integration to the surrounding tissues, clinical manageability, and structural strength in the case of stronger tissues (e.g. bone) [15,18,39–46]. As in other GTR approaches, the inclusion of a membrane could be conducive to the organized regeneration of layers in skin. The membrane should act as a physical barrier for cells, maintaining two populations separated by inhibiting migration from one layer to the other. Simultaneously, the membrane should still be permeable to allow transport of biomolecules such as growth factors, hormones, or nutrients between the two sides. To this end, we proposed the use of keratin-based crosslinked membranes (Fig. 1) and we aimed to prove that dityrosine bonding could be used to engineer their microstructural and transport properties.

### 4.1. The effects of energy density (ED) on the crosslinking density (CD) of keratin membranes

As illustrated in Fig. 1A, riboflavin activation (and formation of reactive species) occurs in the presence of UV light. The tyrosine amino acids in keratin have a susceptible hydroxyl group that can lose its hydrogen to free radical environments, especially in a persulfate radical catalyst like SPS. The tyrosyl radicals formed can bind in pairs forming dityrosine bonds, bridging two keratin chains. When the resin combination is exposed to UV light, riboflavin initiates free radical reactions mediated by the SPS that result in dityrosine crosslinking [32,47,48]. Hydroquinone is an inhibitor of radical-initiated polymerizations, as it is a reducing agent. By using it, the crosslinking reaction is controlled and occurs only when riboflavin initiates under UV.

This chemical sequence was confirmed with the consumption of riboflavin as ED increased (Fig. 2B); sol fraction changes indicated that the structures were being crosslinked to different extents (Fig. 2C). The riboflavin consumption data indicates that there is enough initiator to keep the reaction occurring with at least  $134.4 \text{ mJ/mm}^3$ , yet the sol fraction plot shows that the structure seems to reach crosslinking saturation between  $33.6$  and  $67.2 \text{ mJ/mm}^3$ . These independent sets of data suggest that the limiting reagent in our crosslinking

scheme is not the photoinitiator riboflavin but rather the amount of tyrosine content present in the keratin chains. Even with a wide range of ED, close to 70% of the mass of the hydrogel remained uncrosslinked; this limitation is indicative of the low tyrosine concentration and the amount of bonds available.

Knowing that crosslinking was occurring, FTIR analyses (Fig. 2D) were performed to confirm changes in chemical bonds according to the reaction shown in Fig. 1A. The spectra showed peaks representative of C = C stretch patterns in aromatic rings, such as those found in tyrosine and dityrosine bonds (Fig. 1A). The quantification of the peak magnitudes, which correlates to the amount of dityrosine bonds present, increased with ED until it reached a plateau value at 67.2 mJ/mm<sup>3</sup> (Fig. 2E). These results corroborate the findings of Fig. 2B and C and allow us to determine that i) the dityrosine crosslinking reaction is occurring as designed; ii) the reaction is dependent on the ED, and iii) there is an ED threshold at 67.2 mJ/mm<sup>3</sup> after which crosslinking is maximized because of the limited quantity of tyrosine bonds available. Furthermore, the data indicates that the hydroquinone inhibitor works; without it the free radical reaction would continue in the absence of UV light and all samples would display the same CD.

We were further interested in obtaining a range of CDs that could be tested for molecular transport and a method that can standardize the production of keratin membranes with designed CDs. To this end, we used the thermal method used by Hirschl et al. [34] to measure CD using DSC. In a preliminary calorimetric assessment, TGA profiles of crosslinked samples differed from the unreacted reference; the higher temperatures reached without mass changes are indicative of the formation of bonds that require higher amounts of thermal energy to break (Fig. 2F). The temperature range where these differences occurred was used for DSC testing. The DSC profiles showed a peak characteristic to keratin samples (crosslinked and uncrosslinked). The reduction of this peak as ED increased is indicative of the reduction of available bonding sites as ED increases; available bonding sites are less stable and have higher potential energy than bonded sites, which are portrayed in higher and wider peaks in the thermogram (Fig. 2G and H). The relation between ED and CD is non-linear and mirrors the saturation behavior shown by FTIR data in Fig. 2E. Furthermore, Fig. 2H not only illustrates the ranges and variations of CD for keratin-based hydrogels, but further confirms the threshold ED between 33.6 and 67.2 mJ/mm<sup>3</sup>. Comparison of CD data to other biologically-derived hydrogels is limited as indirect quantifications are generally reported or calculated as theoretical crosslink density (in terms of molarity) [48–50], an approach we had previously reported for the photosensitive resin [32]. Other approaches in literature generally use indirect assessments of the CD degree (using swelling or degradation data, sol fraction, mechanical testing, chemical spectra, etc.) [47,49–54] or crosslinking kinetic models [55,56] to evaluate the CD of biologically-derived polymers. The non-linear relation between CD and ED can be further exploited as a design criterion; using Fig. 2H we can now design the CD of a keratin hydrogel by knowing the required ED. This latter can be then achieved by various combinations of the manufacturing parameters UV intensity ( $I$ ), exposure time ( $t$ ), resin volume ( $V$ ), exposed area ( $A$ ), and sample thickness ( $h$ ).

#### 4.2. Characterization of membrane properties dependent on the network microstructure

Having determined the relation between ED and CD, we proceeded to engineer keratin membranes with different physicochemical properties, such as swelling, degradation, and mechanical behaviors. As presented in Fig. 3A, keratin hydrogels exhibited an initial swelling inversely proportional to the ED of the sample. After 5 days the different groups started diverging and losing their swelling capacities at different rates (Fig. 3A and B). These changes are indicative of ongoing degradation within the keratin network. The high ED groups (over  $67.2 \text{ mJ/mm}^3$ ) showed slower swelling kinetics than groups with low ED, likely due to the higher CD. Swelling was no longer ED-dependent in high ED groups, consistent with the other data sets and the constant CD above  $67.2 \text{ mJ/mm}^3$  of ED (Fig. 2H). As the assay is mass-based, mass loss due to degradation would cause the swelling values to drop. Based on these variations and macroscopic observations, degradation started to occur much faster for low ED groups. This is an important set of data for the engineered membranes; eventually, when subjected to physiological aqueous conditions the hydrogels will undergo “four stages of degradation, namely hydration, strength loss, loss of mass integrity, and solubilization via phagocytosis”[15]. Excluding the last cell-mediated stage, the swelling profiles compiled here provide a clear picture of the behavior that different ED samples would eventually undergo in vivo. Low ED groups will likely undergo higher hydration but also fall into strength loss and loss of mass integrity stages much faster than higher ED groups; furthermore, this can be an indication that low ED groups will be solubilized by phagocytosis faster than their higher ED counterparts. This set of data further proves our bonding threshold identified by sol fraction, riboflavin consumption, FTIR, and DSC assays. Here, we considered that the system reached the maximum CD with  $67.2 \text{ mJ/mm}^3$  of ED, the level at which the swelling capability no longer increased and remained stable at the 1500–2000% range. In comparison, we previously reported the swelling capacity for printed keratin scaffolds at 1581.9% [32], and in both studies it improves the behavior of other similar protein-based hydrogels formed by conventional casting including casted gelatin [57], keratin-collagen scaffolds [58], keratin scaffolds [48], silk fibroin-chitosan scaffolds [50], or DTBP-modified chitosan [49].

Swelling profiles were also used to assess the accuracy of the ED equation proposed (Eq. (1)), by comparing the behavior of duplicated ED samples produced with different combinations of thickness and UV exposure time (Fig. 3C). For example, samples with ED of  $25.2 \text{ mJ/mm}^3$  were produced with combinations 12–1 and 24–2; same for groups  $50.4 \text{ mJ/mm}^3$  (24–1 and 48–2) and  $100.8 \text{ mJ/mm}^3$  (48–1 and 96–2), as highlighted in Fig. 2A with the paired columns. Fig. 3C shows that duplicated groups behave similarly, following very close trends but presenting statistically significant differences. They are close, yet not equal. The ED approach to the production of crosslinked membranes is limited to five variables. These variables were chosen because they are the parameters that we routinely fine-tune during a simple casting process or in stereolithography-based 3D printing. The simplified ED equation proposed adequately incorporates the broader parameters involved in the crosslinking process, but variations in the duplicated groups could be tracked back to more complex properties of the resin. The equation could be further optimized by including parameters such as the optical properties, homogeneity of the material, the penetration and attenuation of UV light through the keratin resin, and the UV absorption by the constituent

molecules of the resin. Other publications have detailed on the effect of various complex parameters in light-based crosslinking, particularly for 3D printing purposes, including the critical energy required to initiate polymerization, the penetration depth of the curing light [59,60], and UV absorption [61]. These reports focused on one or two variables and involved synthetic materials that have been extensively characterized. Other parameters such as initiator concentration, keratin concentration, the shapes and resolution, or cytotoxicity, had been previously studied during the formulation of the resin [32]. The ED parameter proposed does not depend on properties specific to the material but on variables involved in the curing process, and has been proven to be consistent using a highly complex protein-based material such as keratin. Based on the consistency of our results and the cross-examination with a variety of chemical and mechanical assays, the energy density parameter ED can be reliably used to characterize the physicochemical properties of crosslinked membranes (<3 mm thick). It is worth highlighting that any attempts to produce thicker samples (anything thicker than 4–5 mm) should consider expanding the ED equation to include exponential decay parameters that account for the decay of UV light intensity with increasing penetration depth during crosslinking, according to the Beer-Lambert's law. For instance, intensity parameter  $I$  could be replaced by  $\langle I \rangle$ , given by averaged integration of the Beer-Lambert's law over the film thickness.

Furthermore, the swelling profiles provide preliminary information on the degradation of the hydrogels and highlight a potential release limitation of the system. Saul et al. [28] previously discussed the considerable effects of diffusion- and degradation-mediated release from self-assembled keratin hydrogels. As observed in Fig. 3A, decreases in swelling potential could be indicative of degradation and of degradation-mediated release. In this study, the primary goal was to understand the degree of diffusion-mediated release of uncrosslinked components (both uncrosslinked keratin and unreacted chemical resin components), as studied with data such as Fig. 2B and C and 3A and C. Diffusion-mediated release could potentially impact diffusion transport across the membrane; understanding this phenomenon provided a testing time frame when the membranes had no uncrosslinked components leaching or major degradation. This was addressed by implementing a consistent rinsing protocol (Supplementary data and Fig. S1) to remove the bulk of the uncrosslinked components and by using the swelling profiles (Fig. 3A) to determine a time frame (3–5 days) before any ED group presented a significant drop in mass (quantified as swelling degree). With time, which depends on biochemical cues and environmental factors, there will be degradation-mediated release. This scenario will release (1) crosslinked components that are breaking down or are released by bond cleavage, and (2) additional uncrosslinked components trapped within the crosslinked mesh.

Mechanical assessment of the membranes revealed the effect of ED on the compressive moduli and ultimate stress and strain of the keratin materials. The data correlates to the crosslinking dynamics of the system. Even if the energy delivered can keep increasing, the crosslink bonds are dependent on the available tyrosine, and thus it reaches a maximum CD and maximum structural properties. On one hand, swelling data indicates that the system is reaching the maximum capacity with  $67.2 \text{ mJ/mm}^3$  of energy, a level at which swelling is significantly more stable (Fig. 3A and B). On the other, the elastic moduli and ultimate stress and strain registered for samples with ED below  $67.2 \text{ mJ/mm}^3$  show a significantly

increasing trend, indicating they are within a range of variable CD (Fig. 3D and E). Overall, the swelling and mechanical profiles and the data compiled from them confirm our expectations of the UV-photosensitive chemistry and its saturation, and again confirm the ED threshold. We discussed the limitations of the ED parameter proposed, but the behavior in swelling and mechanical properties indicate that the keratin membranes can be fine-tuned over wide ranges using our simplified ED approach. It is worth highlighting again that the goal of this section was to prove that the ED parameter, which defines CD, can be used to produce keratin membranes with a variety of properties, including a wide range of swelling profiles, degradation behaviors, mechanical properties, and diffusion capabilities. Here, we present a range of options to our fellow researchers with the interest of showing the versatility of our ED approach and the membranes produced. Hydrogels produced with low ED might be suitable for applications interested in fast release, such as the studies of Saul et al. [28] for the sustained release of bioactive ciprofloxacin from keratin hydrogels, while we expect to use the high ED hydrogels for sustained use as membranes that should have lower effects on diffusion applications.

#### **4.3. The effects of crosslink degree (CD) on transport phenomena across keratin membranes**

The use of the keratin-based crosslinked hydrogels as membranes was proposed based on the criteria that it should 1) act as a physical barrier for cells so that two populations can grow adjacently without mixing; 2) be permeable to allow transport of biomolecules to allow cross-talk between the two layers; and 3) it should be able to degrade as the layers form, without leaching cytotoxic by-products or having major impact on skin properties such as water transport, elasticity, or scarring. Here, we focused on studying the second criterion using membranes with a range of CD that would impact molecular transport of model molecules, growth factors, and nutrients across the hydrogel (Fig. 4A).

Hydrogels were successfully implemented as membranes using Transwell inserts with the addition of 3D printed stoppers, which allowed sealing and ensured that all diffusion occurred through the membrane.  $K$  was determined by the size of the FITCd molecules in solution, but it was further affected by the ED of the membranes. As defined in Eq. (3),  $K$  is the ratio between the concentrations of solute in the hydrogel and in solution. In a balanced gel-solution system, half of the solute would theoretically localize in the gel and half in the solution. The smaller 10 kDa groups resulted in an unbalanced system where most of the solute was uptaken by the hydrogel ( $K > 0.5$ ); the larger 2000 kDa groups were also unbalanced, although the majority of the FITCd molecules remained in solution ( $K < 0.5$ ). The 150 kDa molecules seemingly reached a balanced state of equilibrium, where the solute was closely equally distributed between gel and solution ( $K \approx 0.5$ ). This indicates that smaller molecules are uptaken and retained within the membranes even against a concentration gradient.

The partition coefficient and permeability studies using FITCd elucidated on the effect of membrane design properties, mainly ED and CD, on the transport of different-sized molecules (Fig. 4B and C). In general, taking the increasing trends between  $K$  and ED for all MWs, the higher ED allows higher uptake of solutes into the hydrogel. At any particular

time the low MW samples are more uptaken by the hydrogels (K of up to 0.8) than the higher MW samples (maximum 0.3 and 0.5) no matter the ED. On the other hand, P increases as ED increases for the high MW. K is the property in equilibrium, while P is the product of the equilibrium (how much solute is uptaken and remains in the gel) and the dynamic transport (how much solute moves across the hydrogel). When pairing both sets of data we can conclude that for the low MW higher amounts of solute are accumulated within the keratin gel, a trend that does not change with increasing ED. This indicates the low MW samples remain within the membranes. On the other hand, larger molecules present higher P and lower K values through the gels which are indicative of transport across the barrier. For these, the effect of the ED of the membranes is clearer. As the ED of the membrane increases the P and K values also increase, indicating that increasing ED does represent better diffusion rates through the membrane. In terms of molecule size and shape, the Stoke's radii for FITCd 10, 150, and 2000 kDa is reported as approximately 23, 85, and 270 Angstroms, respectively [62,63]. Low MW FITCd (below 2 kDa) is rod-like, while chains with 2 to 10 kDa behave like flexible coils. FITCd larger than 10 kDa behaves as highly branched polymers and become increasingly symmetrical [62,63]. The size and shape indicate that the smaller molecules might be interacting chemically or electrostatically with the networks or are trapped within the smaller pores of the hydrogel. The larger molecules, due to their size and flexibility, are probably crossing the hydrogel via the larger pores, slower but without interaction or entrapment. Low CD membranes, which present lower values of P, may have unreacted portions within their chains that can be responsible of reducing transport; as the CD increases, interaction between the chains and the molecules is reduced, allowing higher transport rates.

The transport of molecules across the membrane was further studied with the diffusion of adipogenic molecules for the differentiation of a target hMSC population. The healthy development of the adipose layer (hypodermis) in severe burn wounds is of particular interest. This is a rich layer of adipocytes and stem cells that synthesize adipose-specific ECM (mostly collagen types I, III, IV, V, and VI [64]) and growth factors (highlighting leptin [21,65] and adiponectin [66,67] hormones, and basic fibroblast growth factor [68]) key players in re-epithelization, wound healing, and angiogenesis [64]. If the hypodermis is producing all these factors *in vivo*, diffusion through the tissues is transporting them to the adjacent dermis layer. Ensuring the transport of biomolecules across keratin membranes will further help us to eventually replicate the transport between stratified hypodermis and dermis to prove its benefits in regeneration of skin. As presented in Fig. 4D and E, the membranes with higher CD (55, 59%) allowed transport of molecules involved in adipogenic differentiation that resulted in higher lipid deposition, in comparison to the 20 and 47% CD groups. Formation of intracellular lipid droplets are evidence that adipogenic factors were transported; some combination of the growth factors, hormones, amino acids, vitamins, sugars, and steroids found in the DMEM, FBS, P/S, sodium pyruvate, dexamethasone, insulin, IBMX, and indomethacin that make up the adipogenic media, were able to cross the membrane and reach the cells to induce adipogenic differentiation. Similar to behavior observed in the P and K experiments, some fraction of the adipogenic molecules is always transported as no membrane proved to fully inhibit molecular transport, a fact backed by all membranes allowing differentiation of the cells (as compared to a

nomembrane scenario). Considering that the differentiation of hMSCs is a delicate process that requires a very specific combination of the components mentioned before, we can assume that the differentiation observed is the result of all, or most, molecules being able to cross the membranes. Based on our characterization (FTIR, DSC crosslinking density, and the quantification of structural and diffusion properties), there is a marked difference with membranes produced with ED below the 67.2 mJ/mm<sup>3</sup> threshold. At that ED level, all results indicate that the membranes have reached a maximum level of crosslinking (CD of 55–59%); over this ED threshold, the membranes allow better transport of growth factors that result in improved adipogenic differentiation of hMSCs.

## 5. Conclusions

The goal of this work was to develop a GTR-based membrane with engineered microstructural and transport properties for future use in the development of stratified tissues. We introduced an energy density (ED) parameter that incorporates simplified casting and printing parameters for the sequential production of thin keratin-based membranes. Our keratin-based resin has been optimized for the reproducible manufacture of membranes with defined CD and physicochemical properties, which correlate to the ED level selected. Keratin membranes allow diffusion of molecules such as media nutrients and growth factors, and the ED of the crosslinked network can be used to regulate the transport profiles. Further studies are warranted to quantify the cross-talk between cell populations across the membrane, evaluate the barrier effect of the membranes on cell migration, and the *in vivo* development of dermal layers. Overall, we can now engineer and manufacture our membranes and conclude that fine tuning the CD is valuable to control several microstructural properties of the hydrogels, including swelling and degradation profiles, mechanical properties, and transport across the network.

## Supplementary Material

Refer to Web version on PubMed Central for supplementary material.

## Acknowledgements

The authors gratefully acknowledge the collaboration of KeraNetics, LLC, as the developers of the keratin extraction process and the providers of raw material used here. This research was supported by the National Institute of Biomedical Imaging and Bioengineering/National Institutes of Health (NIBIB/NIH) Center for Engineering Complex Tissues (P41 EB023833). This project is based upon work supported by USAMRAA under Contract No. W81XWH-14-C-0022. Opinions, findings and conclusions or recommendations expressed here are those of the author(s) and do not necessarily reflect the views of USAMRAA. The authors thank the Fulbright Scholars Program (JN), NIST grant 2014-NIST-MSE-01 (MJL), and SEEDS Undergraduate Research program at the University of Maryland (JS). The authors gratefully acknowledge Mr. Patrick Stanley (UMD Energy Research Center) for his help with their TGA system.

## References

- [1]. World Health Organization (WHO), “Burns: Fact Sheet (Reviewed September 2016).” 2016.
- [2]. Markeson D, Pleat JM, Sharpe JR, Harris AL, Seifalian AM, Watt SM, Scarring, stem cells, scaffolds and skin repair, *J. Tissue Eng. Regen. Med.* 9 (6) (2015) 649–668. [PubMed: 24668923]
- [3]. Atiyeh BS, Gunn SWA, Hayek SN, Military and civilian burn injuries during armed conflicts, *Ann. Burns Fire Disasters* 20 (4) (2007) 203–215. [PubMed: 21991098]

- [4]. Weiss J, Women's rights in Colombia: Acid attacks on the rise, *World Aff.* 177 (2) (2014) 50–57.
- [5]. Mannan A, Ghani S, Sen SL, Clarke A, Butler PEM, The problem of acid violence in Bangladesh, *J. Surg* 2 (1) (2004) 39–43.
- [6]. Seifert D, Krohn J, Larson M, Lambe A, Püschel K, Kurth H, Violence against children: further evidence suggesting a relationship between burns, scalds, and the additional injuries, *Int. J. Legal Med.* 124 (1) (2010) 49–54. [PubMed: 19399513]
- [7]. American Burn Association, “National Burn Awareness Week 2017 Fact Sheet.” 2017.
- [8]. Peck M, Molnar J, Swart D, A global plan for burn prevention and care, *Bull. World Health Organ.* 87 (10) (2009) 802–803. [PubMed: 19876549]
- [9]. Böttcher-Haberzeth S, Biedermann T, Reichmann E, Tissue engineering of skin, *Burns* 36 (4) (Jun. 2010) 450–460. [PubMed: 20022702]
- [10]. Hu MS, Maan ZN, Wu J-C, Rennert RC, Hong WX, Lai TS, Cheung ATM, Walmsley GG, Chung MT, McArdle A, Longaker MT, Lorenz HP, Tissue engineering and regenerative repair in wound healing, *Ann. Biomed. Eng* 42 (7) (2014) 1494–1507. [PubMed: 24788648]
- [11]. World Health Organization (WHO), “Burn Prevention: Success Stories, Lessons Learned,” 2011.
- [12]. Orgill DP, Ogawa R, Current methods of burn reconstruction, *Plast. Reconstr. Surg* 131 (5) (2013) 827e–836e.
- [13]. Jansen J.a., de Ruijter JE, Janssen PT, Paquay YG, Histological evaluation of a biodegradable Polyactive/hydroxyapatite membrane, *Biomaterials* 16 (11) (1995) 819–827. [PubMed: 8527596]
- [14]. Nieminen T, Kallela I, Keränen J, Hiidenheimo I, Kainulainen H, Wuolijoki E, Rantala I, In vivo and in vitro degradation of a novel bioactive guided tissue regeneration membrane, *Int. J. Oral Maxillofac. Surg* 35 (8) (2006) 727–732. [PubMed: 16569496]
- [15]. Retzepi M, Donos N, Guided Bone Regeneration: biological principle and therapeutic applications, *Clin. Oral Implants Res* 21 (6) (2010) 567–576. [PubMed: 20666785]
- [16]. Thoma DS, Halg GA, Dard MM, Seibl R, Hammerle CHF, Jung RE, Evaluation of a new biodegradable membrane to prevent gingival ingrowth into mandibular bone defects in minipigs, *Clin. Oral Implants Res* 20 (1) (2009) 7–16. [PubMed: 19126102]
- [17]. Yang F, Both SK, Yang X, Walboomers XF, Jansen JA, Development of an electrospun nano-apatite/PCL composite membrane for GTR/GBR application, *Acta Biomater* 5 (9) (2009) 3295–3304. [PubMed: 19470413]
- [18]. Cai Y, Guo J, Chen C, Yao C, Chung SM, Yao J, Lee IS, Kong X, Silk fibroin membrane used for guided bone tissue regeneration, *Mater. Sci. Eng. C* 70 (2017) 148–154.
- [19]. Hill P, Brantley H, Van Dyke M, Some properties of keratin biomaterials: Kerateines, *Biomaterials* 31 (4) (2010) 585–593. [PubMed: 19822360]
- [20]. Gillespie JM, Proteins rich in glycine and tyrosine from keratins, *Comp. Biochem. Physiol. Part B Biochem* 41 (4) (1972).
- [21]. Kolarsick PAJ, Kolarsick MA, Goodwin C, Anatomy and physiology of the skin, *J. Dermatol. Nurses. Assoc* 3 (4) (Jul. 2011) 203–213.
- [22]. Loan F, Cassidy S, Marsh C, Simcock J, Keratin-based products for effective wound care management in superficial and partial thickness burns injuries, *Burns* 42 (3) (5 2016) 541–547. [PubMed: 26787130]
- [23]. Tomblin S, Pettit Kneller EL, Walker SJ, Ellenburg MD, Kowalczewski CJ, Van Dyke M, Burnett L, Saul JM, Keratin hydrogel carrier system for simultaneous delivery of exogenous growth factors and muscle progenitor cells, *J. Biomed. Mater. Res. – Part B Appl. Biomater.* 104 (5) (2016) 864–879. [PubMed: 25953729]
- [24]. Sierpinski P, Garrett J, Ma J, Apel P, Klorig D, Smith T, Koman LA, Atala A, Van Dyke M, The use of keratin biomaterials derived from human hair for the promotion of rapid regeneration of peripheral nerves, *Biomaterials* 29 (1) (2008) 118–128. [PubMed: 17919720]
- [25]. Verma V, Verma P, Ray P, Ray AR, “Preparation of scaffolds from human hair proteins for tissue-engineering applications, *Biomed. Mater* 3 (2) (2008).
- [26]. Pace LA, Plate JF, Smith TL, Van Dyke ME, The effect of human hair keratin hydrogel on early cellular response to sciatic nerve injury in a rat model, *Biomaterials* 34 (24) (2013) 5907–5914. [PubMed: 23680369]

- [27]. Nayak KK, Gupta P, In vitro biocompatibility study of keratin/agar scaffold for tissue engineering, *Int. J. Biol. Macromol* 81 (2015) 1–10. [PubMed: 26188296]
- [28]. Saul JM, Ellenburg MD, De Guzman RC, Van Dyke M, Keratin hydrogels support the sustained release of bioactive ciprofloxacin, *J. Biomed. Mater. Res. - Part A* 98 A (4) (2011) 544–553.
- [29]. Nakata R, Tachibana A, Tanabe T, Preparation of keratin hydrogel/ hydroxyapatite composite and its evaluation as a controlled drug release carrier, *Mater. Sci. Eng. C* 41 (2014) 59–64.
- [30]. Xu S, Sang L, Zhang Y, Wang X, Li X, Biological evaluation of human hair keratin scaffolds for skin wound repair and regeneration, *Mater. Sci. Eng. C* 33 (2) (2013) 648–655.
- [31]. Poranki D, Whitener W, Howse S, Mesen T, Howse E, Burnell J, GreengauzRoberts O, Molnar J, Van Dyke M, Evaluation of skin regeneration after burns invivo and rescue of cells afterthermal stress invitro following treatment witha keratin biomaterial, *J. Biomater. Appl* 29 (1) (Jul. 2014) 26–35. [PubMed: 24272161]
- [32]. Placone JK, Navarro J, Laslo GW, Lerman MJ, Gabard AR, Herendeen GJ, Falco EE, Tomblyn S, Burnett L, Fisher JP, Development and Characterization of a 3D Printed, Keratin-Based Hydrogel, *Ann. Biomed. Eng* 45 (1) (2017) 237–248. [PubMed: 27129371]
- [33]. Menges F, “Spectragryph – Software for optical spectroscopy.” 2017.
- [34]. Hirschl C, Biebl-Rydlo M, Debiasio M, Mühleisen W, Neumaier L, Scherf W, Oreski G, Eder G, Chernev B, Schwab W, Kraft M, Determining the degree of crosslinking of ethylene vinyl acetate photovoltaic module encapsulants – a comparative study, *Sol. Energy Mater. Sol. Cells* 116 (2013) 203–218.
- [35]. Lazzara MJ, Deen WM, Effects of concentration on the partitioning of macromolecule mixtures in agarose gels, *J. Colloid Interface Sci.* 272 (2) (2004) 288–297. [PubMed: 15028489]
- [36]. Cussler EL, *Diffusion, Mass Transfer in Fluid Systems*, 3rd ed., Cambridge University Press, Cambridge, 2009.
- [37]. Wexler SA, Donaldson C, Denning-Kendall P, Rice C, Bradley B, Hows JM, Adult bone marrow is a rich source of human mesenchymal ‘stem’ cells but umbilical cord and mobilized adult blood are not, *Br. J. Haematol* 121 (2) (2003) 368–374. [PubMed: 12694261]
- [38]. Yang Z, Schmitt JF, Lee EH, Immunohistochemical analysis of human mesenchymal stem cells differentiating into chondrogenic, osteogenic, and adipogenic lineages, *Methods* 698 (5) (2011) 353–366.
- [39]. Hunter KT, Ma T, “In vitro evaluation of hydroxyapatite-chitosan-gelatin composite membrane in guided tissue regeneration, *J. Biomed. Mater. Res. - Part A* 101A (4) (2013) 1016–1025.
- [40]. Hurt AP, Getti G, Coleman NJ, Bioactivity and biocompatibility of a chitosantobermorite composite membrane for guided tissue regeneration, *Int. J. Biol. Macromol* 64 (2014) 11–16. [PubMed: 24296410]
- [41]. Bottino MC, Thomas V, Janowski GM, A novel spatially designed and functionally graded electrospun membrane for periodontal regeneration, *Acta Biomater.* 7 (1) (2011) 216–224. [PubMed: 20801241]
- [42]. Gürbüz S, Demirtas TT, Yüksel E, Karakeçili A, Doğan A, Gümüsderelioğlu M, Multi-layered functional membranes for periodontal regeneration: Preparation and characterization, *Mater. Lett* 178 (2016) 256–259.
- [43]. Jamuna-Thevi K, Saarani NN, Abdul Kadir MR, Hermawan H, Triple-layered PLGA/ nanoapatite/lauric acid graded composite membrane for periodontal guided bone regeneration, *Mater. Sci. Eng. C* 43 (2014) 253–263.
- [44]. Xue J, He M, Niu Y, Liu H, Crawford A, Coates P, Chen D, Shi R, Zhang L, Preparation and in vivo efficient anti-infection property of GTR/GBR implant made by metronidazole loaded electrospun polycaprolactone nanofiber membrane, *Int. J. Pharm* 475 (1) (2014) 566–577. [PubMed: 25240438]
- [45]. Xue J, Shi R, Niu Y, Gong M, Coates P, Crawford A, Chen D, Tian W, Zhang L, Fabrication of drug-loaded anti-infective guided tissue regeneration membrane with adjustable biodegradation property, *Colloids Surfaces B Biointerfaces* 135 (2015) 846–854. [PubMed: 25847456]
- [46]. Li H, Song P, Qiao T, Cui Q, Song X, Zhang B, A quaternary composite fiber membrane for guided tissue regeneration, *Polym. Adv. Technol* 27 (2) (2016) 178–184.

- [47]. Vashi AV, Werkmeister JA, Vuocolo T, Elvin CM, Ramshaw JAM, Stabilization of collagen tissues by photocrosslinking, *J. Biomed. Mater. Res. Part A* 100 A (9) (2012) n/a-n/a.
- [48]. Sando L, Kim M, Colgrave ML, Ramshaw JAM, Werkmeister JA, Elvin CM, Photochemical crosslinking of soluble wool keratins produces a mechanically stable biomaterial that supports cell adhesion and proliferation, *J. Biomed. Mater. Res. Part A* 95A (3) (Dec. 2010) 901–911.
- [49]. Adekogbe I, Ghanem A, Fabrication and characterization of DTBP-crosslinked chitosan scaffolds for skin tissue engineering, *Biomaterials* 26 (35) (2005) 7241–7250. [PubMed: 16011846]
- [50]. Zhang X, Jia C, Qiao X, Liu T, Sun K, Silk fibroin microfibers and chitosan modified poly (glycerol sebacate) composite scaffolds for skin tissue engineering, *Polym. Test* 62 (2017) 88–95.
- [51]. Melchiorri AJ, Hibino N, Best C.a., Yi T, Lee YU, Kraynak C.a., Kimerer LK, Krieger a., Kim P, Breuer CK, Fisher JP, 3D-printed biodegradable polymeric vascular grafts, *Adv. Healthc. Mater* 5 (3) (2016) 319–325. [PubMed: 26627057]
- [52]. Malencik DA, Sprouse JF, Swanson CA, Anderson SR, Dityrosine: preparation, isolation, and analysis, *Anal. Biochem* 242 (2) (1996) 202–213. [PubMed: 8937563]
- [53]. Dijkgraaf LC, Zardeneta G, Cordewener FW, Liem RSB, Schmitz JP, De Bont LGM, Milam SB, Crosslinking of fibrinogen and fibronectin by free radicals: a possible initial step in adhesion formation in osteoarthritis of the temporomandibular joint, *J. Oral Maxillofac. Surg* 61 (1) (2003) 101–111. [PubMed: 12524616]
- [54]. Scott McCall A, Kraft S, Edelhauser HF, Kidder GW, Lundquist RR, Bradshaw HE, Dedeic Z, Dionne MJC, Clement EM, Conrad GW, Mechanisms of corneal tissue cross-linking in response to treatment with topical riboflavin and Long-Wavelength Ultraviolet Radiation (UVA), *Investig. Ophthalmol. Vis. Sci* 51 (1) (2010) 129–138. [PubMed: 19643975]
- [55]. Lattuada M, Del Gado E, Abete T, De Arcangelis L, Lazzari S, Diederich V, Storti G, Morbidelli M, Kinetics of free-radical cross-linking polymerization: comparative experimental and numerical study, *Macromolecules* 46 (15) (2013) 5831–5841.
- [56]. Fuxman AM, McAuley KB, Schreiner LJ, Modeling of Free-radical Crosslinking Copolymerization of Acrylamide and N, N0-Methylenebis (acrylamide) for Radiation Dosimetry, *Macromol. Theory Simulations* 12 (9) (2003) 647–662.
- [57]. Elvin CM, Vuocolo T, Brownlee AG, Sando L, Huson MG, Liyou NE, Stockwell PR, Lyons RE, Kim M, Edwards GA, Johnson G, McFarland GA, Ramshaw JAM, Werkmeister JA, A highly elastic tissue sealant based on photopolymerised gelatin, *Biomaterials* 31 (32) (2010) 8323–8331. [PubMed: 20674967]
- [58]. Balaji S, Kumar R, Sripriya R, Rao U, Mandal A, Kakkar P, Reddy PN, Sehgal PK, Characterization of keratin-collagen 3D scaffold for biomedical applications, *Polym. Adv. Technol* 23 (3) (2012) 500–507.
- [59]. Bennett J, Measuring UV curing parameters of commercial photopolymers used in additive manufacturing, *Addit. Manuf* 18 (2017) 203–212. [PubMed: 29503807]
- [60]. Steyrer B, Neubauer P, Liska R, Stampfl J, Visible light photoinitiator for 3Dprinting of tough methacrylate resins, *Materials (Basel)* 10 (12) (2017) 1–11.
- [61]. Seo H, Heo SG, Lee H, Yoon H, Preparation of PEG materials for constructing complex structures by stereolithographic 3D printing, *RSC Adv.* 7 (46) (2017) 28684–28688.
- [62]. Sigma, “Fluorescein Isothiocyanate-Dextran Product Information.” pp. 1–3, 1997.
- [63]. Tdb Consultancy, “FITC-Dextran Fluorescein isothiocyanate dextran.” pp. 1–5, 2010.
- [64]. Kang JH, Gimble JM, Kaplan DL, In vitro 3D model for human vascularized adipose tissue, *Tissue Eng. Part A* 15 (8) (2009) 2227–2236. [PubMed: 19207036]
- [65]. Wong R, Geyer S, Weninger W, Guimberteau JC, Wong JK, The dynamic anatomy and patterning of skin, *Exp. Dermatol* 25 (2) (2016) 92–98. [PubMed: 26284579]
- [66]. Shibata S, Tada Y, Asano Y, Hau CS, Kato T, Saeki H, Yamauchi T, Kubota N, Kadowaki T, Sato S, Adiponectin regulates cutaneous wound healing by promoting keratinocyte proliferation and migration via the ERK signaling pathway, *J. Immunol* 189 (6) (2012) 3231–3241. [PubMed: 22904306]
- [67]. Salathia NS, Shi J, Zhang J, Glynne RJ, An in vivo screen of secreted proteins identifies adiponectin as a regulator of murine cutaneous wound healing, *J. Invest. Dermatol* 133 (3) (2013) 812–821. [PubMed: 23096717]

- [68]. Hebert TL, Wu X, Yu G, Goh BC, Halvorsen Y-DC, Wang Z, Moro C, Gimble JM, Culture effects of epidermal growth factor (EGF) and basic fibroblast growth factor (bFGF) on cryopreserved human adipose-derived stromal/stem cell proliferation and adipogenesis, *J. Tissue Eng. Regen. Med* 3 (7) (Oct. 2009) 553–561. [PubMed: 19670348]

Author Manuscript

Author Manuscript

Author Manuscript

Author Manuscript

## 6. Statement of significance

GTR is a widely used technique for the surgical reconstruction of periodontal and bone defects which relies on membranes that regulate cellular migration and allow the regeneration of complex, specialized tissue microstructures. Here, we developed a method for the production and assessment of protein-based degradable membranes based on the energy delivered to the membranes during crosslinking. We can now engineer the crosslinking density of our membranes and thus their mechanical, swelling, and transport properties. The keratin membranes presented here will allow us to implement the GTR approach to the regeneration of the layered microstructure of skin, a technique that provides physiological regeneration of skin functions as well as aesthetical reconstructions of complex features.

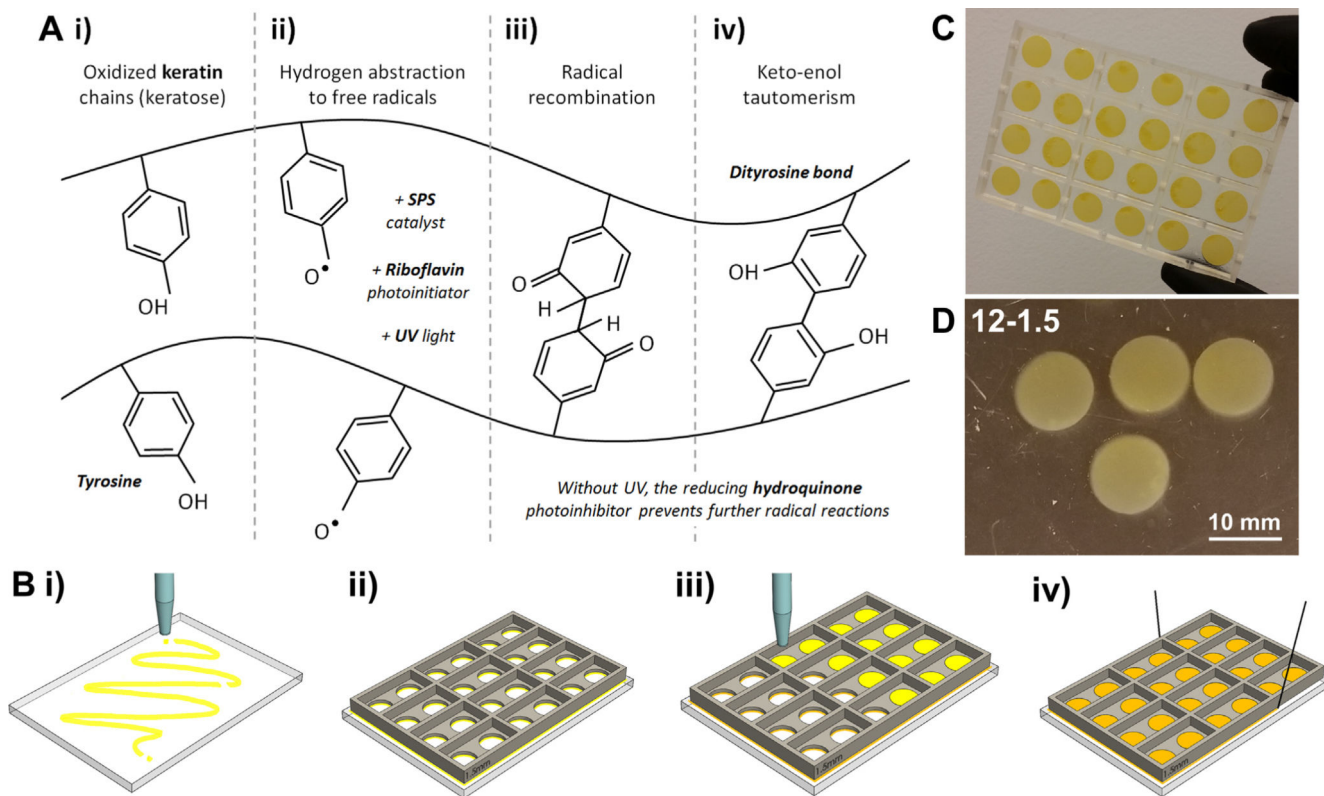


**Fig. 1.** Photocrosslinking of keratin membranes. A) Chemical mechanism for dityrosine bonding in oxidized keratin: i) keratose contains tyrosine within their peptide chains; ii) tyrosine has a susceptible hydroxyl group that be deprotonated upon interaction with free radicals formed between SPS and riboflavin upon UV exposure; iii) unbalanced terminals bond and recombine with unbalanced terminals in adjacent chains; iv) final chemical equilibrium is reached via keto-enol tautomerism when dityrosine bonds between keratin chains are stable; the crosslinking reaction is terminated once removed from a UV source due to the reducing effect of the hydroquinone photoinhibitor. B) Dityrosine chemistry was used to cast keratin membranes: i) a translucent sheet was covered with a thin layer of resin; ii) the casting mold was then laid over the flat sheet and the two were clamped together. The clamped setup was then crosslinked under UV to seal them together; iii) the sealed molds were filled with keratin resin as needed and exposed to UV; iv) the cured mold can be cut from the base sheet using fine thread. C) Examples of crosslinked circular samples 13 mm in diameter with different thicknesses (1, 1.5, or 2 mm). D) Final crosslinked samples 12–1.5 (exposure time 12 min, thickness 1.5 mm) stored in PBS

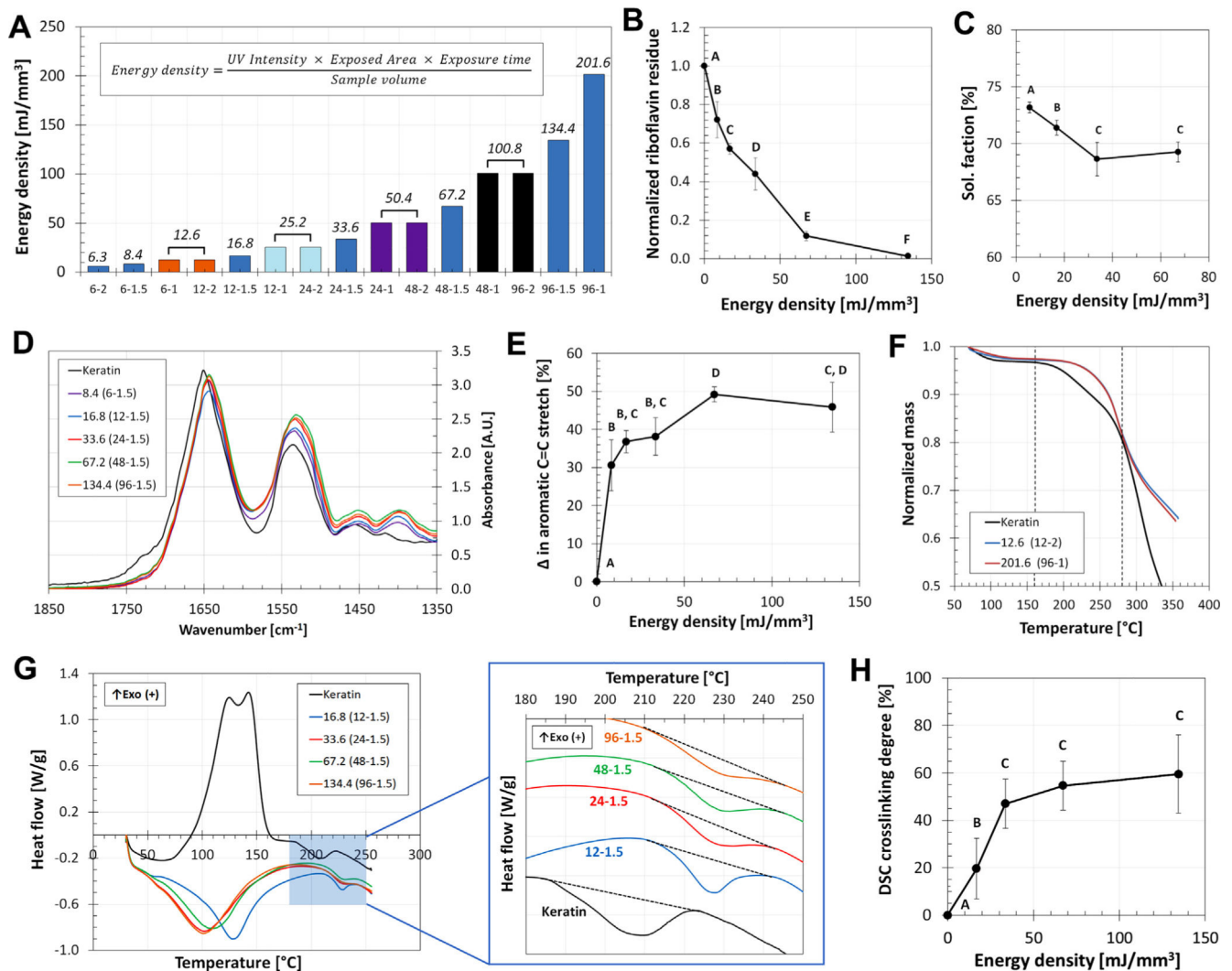


**Fig. 2.** The effects of energy density (ED) on the crosslinking density (CD) of keratin membranes. A) The ED parameter was used to produce a wide range of samples by combining thicknesses and exposure times at a fixed UV intensity of 350 mW/dm<sup>2</sup>. Bars that share the same color were produced with different parameter combinations but have the same ED (listed on top on each bar). The consumption of riboflavin (B) and the sol fraction of the hydrogels (C) confirmed that the crosslinking reaction (Fig. 1A) occurs and is ED-dependent. D) FTIR spectra shows four peaks between 1400 and 1650 cm<sup>-1</sup>, indicative of changes in aromatic structures, that increasing for the higher ED samples. E) The area under the FITR peaks for the samples was normalized against the area under the peaks for unreacted keratin; this quantification shows the change in aromatic C = C stretch between samples and its relation to ED. F) TGA profiles for comparison of crosslinked and uncrosslinked keratin, indicating the formation of bonds and changes in the profiles between 150 and 275 °C. G) DSC thermograms for keratin presents a characteristic peak at 210 °C which changes in magnitude in crosslinked samples (blue region). Organized curves can be further compared to show how the peak shifts to 220–230 °C and varies depending on the

ED of the sample; low energy samples present a defined peak, which progressively decreases as the energy density increases. H) Quantification of these peaks can be related to changes in the enthalpy of the system, indicative of the formation of bonds and the crosslinking degree of the network dependent on the ED. For all plots, samples that do not share the same letter are significantly different ( $p < 0.05$ ). (For interpretation of the references to color in this figure legend, the reader is referred to the web version of this article.)

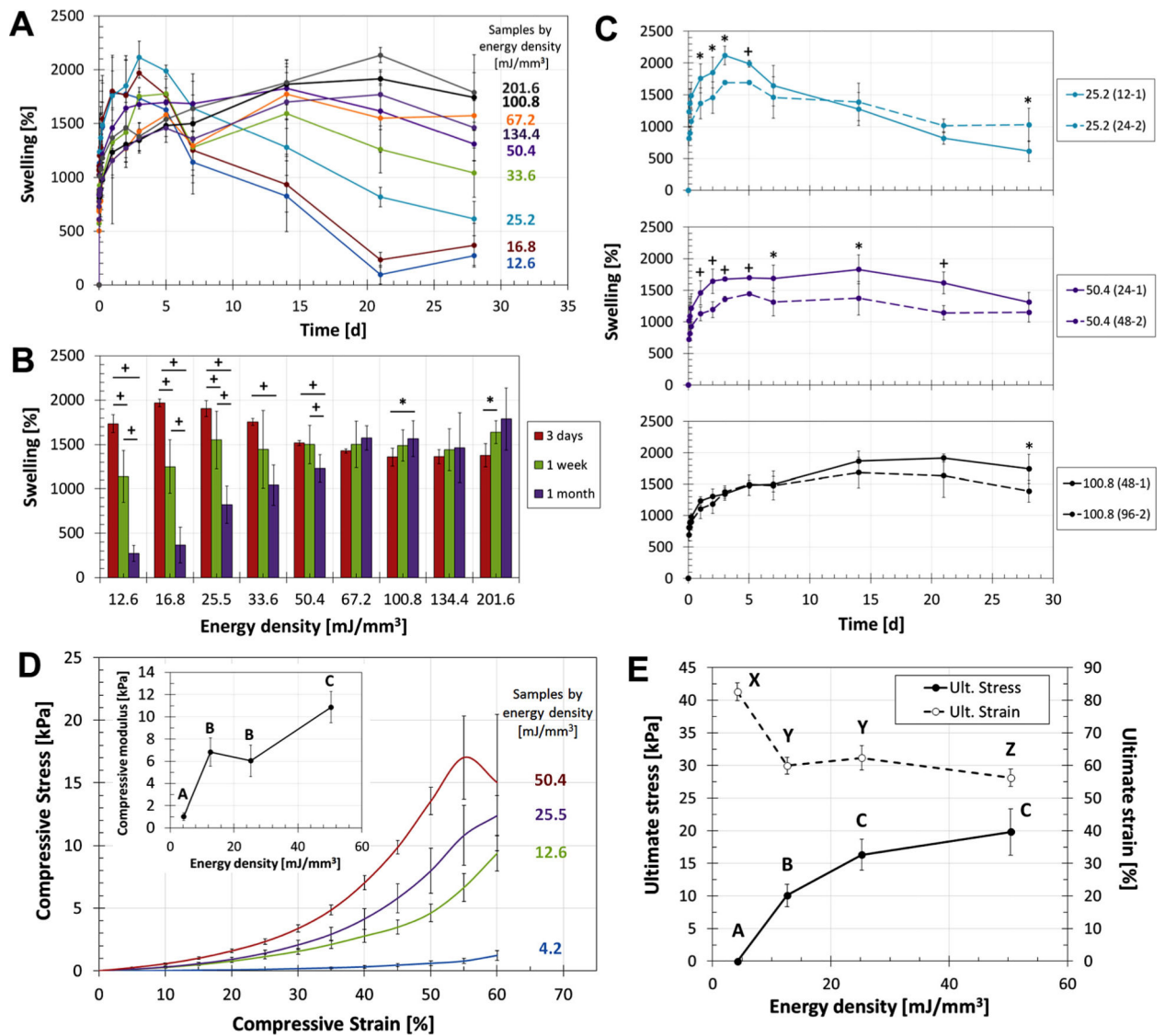


**Fig 3.** Characterization of membrane properties dependent on the network microstructure. A) Swelling profiles of keratin hydrogels in MEM as a function of ED, showing how low ED samples reach their swelling saturation capacity faster than high ED groups yet they also start a process of degradation at earlier timepoints. B) The drop in swelling capacity between days 3 and 28 are indicative of degradation for low ED groups; high ED samples were proven to be highly stable when crosslinked with at least  $67.2 \text{ mJ}/\text{mm}^3$ . C) Different combinations of thickness and exposure time were used to produce duplicated ED values to assess the viability of the ED parameter as proposed in Eq. (1). Even if the duplicates follow close trends, statistical differences indicate that higher complexity in the equation is required (statistical significance  $p < 0.01$  (+) or  $p < 0.05$  (\*)). D-E) Mechanical characterization of the hydrogels shows the relation between ED and elastic modulus, ultimate stress, and ultimate strain., Higher ED samples have higher mechanical properties, following non-linear trends that show a saturation profile that further elucidates on the crosslinking limitations

and maximum capacities. For all plots, samples that do not share the same letter are significantly different ( $p < 0.05$ ).

Author Manuscript

Author Manuscript

Author Manuscript

Author Manuscript

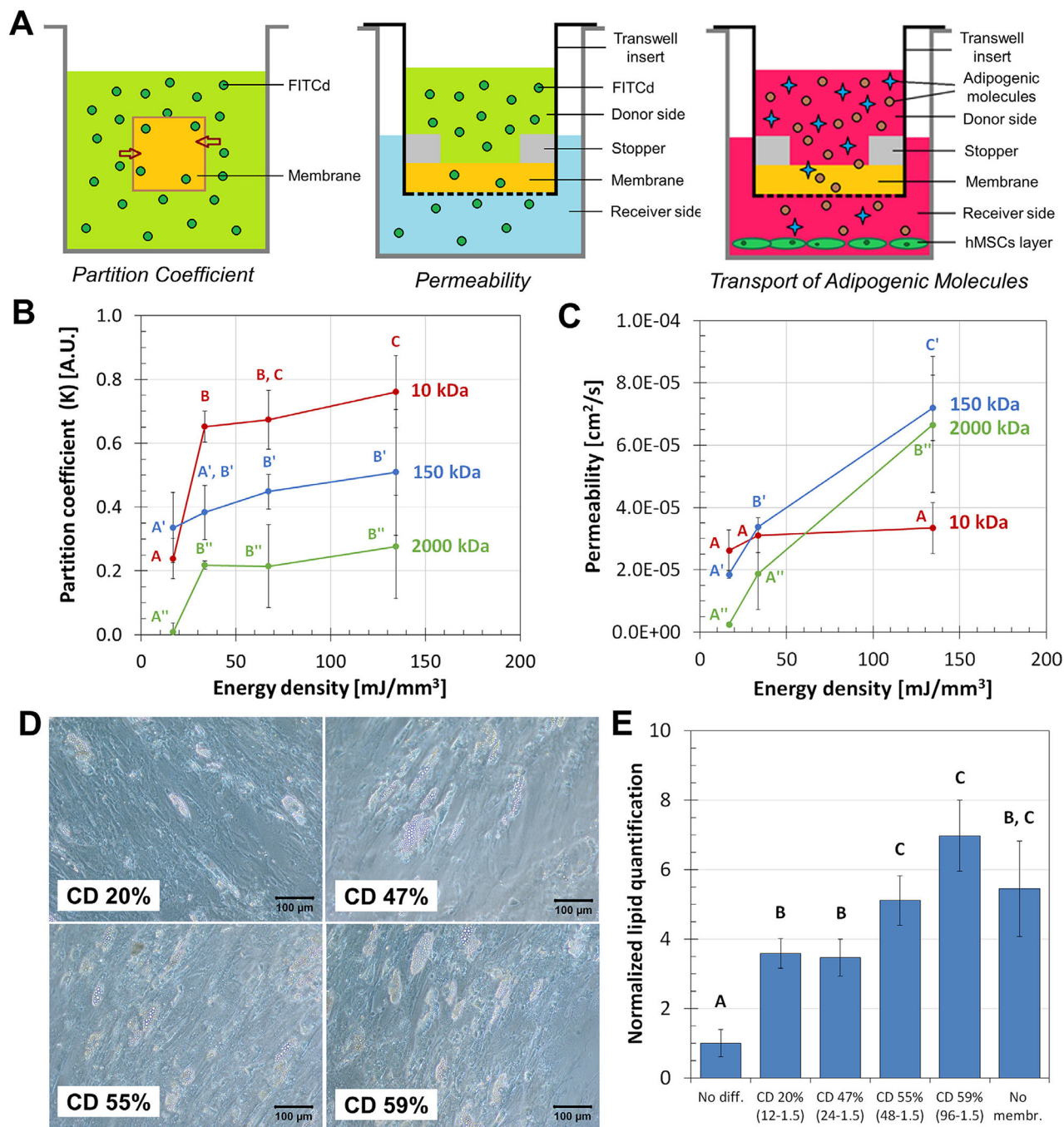


**Fig. 4.** The effects of crosslink degree (CD) on transport phenomena across keratin membranes. A) Transport phenomena across the keratin membranes were studied using simplified models of the partition coefficient, permeability, and diffusion transport of adipogenic molecules. B) The partition coefficient of keratin hydrogels in equilibrium state with 10, 150, and 2000 kDa FITC-d solutions; ED had greater significant effect on the coefficient for smaller molecules. C) Permeability, on the other hand, is the dynamic interaction of the gel with the solute and was affected by ED for the high MW molecules. D-E) Adipogenic differentiation

of hMSCs was significantly affected by the variation of the CD of the membranes used. Imaging and quantification of intracellular lipids determined that membranes with higher CD allow better transport of nutrients and adipogenic molecules after 28 d. For all plots, samples that do not share the same letter are significantly different ( $p < 0.05$ ).